JACS
JOURNAL OF THE AMERICAN CHEMICAL SOCIETY

ARTICLE

pubs.acs.org/JACS

Impact of Molecular Flexibility on Binding Strength and Self-Sorting of Chiral π-Surfaces

Marina M. Safont-Sempere,[†] Peter Osswald,[†] Matthias Stolte,[†] Matthias Grüne,[†] Manuel Renz,[‡] Martin Kaupp,[‡] Krzysztof Radacki,[§] Holger Braunschweig,[§] and Frank Würthner*[,†]

[†]Universität Würzburg, Institut für Organische Chemie and Röntgen Research Center for Complex Material Systems, Am Hubland, 97074 Würzburg, Germany

[‡]Institut für Chemie, Theoretische Chemie, Technische Universität Berlin, Sekr. C 7, Strasse des 17. Juni 135, 10623 Berlin, Germany

[§]Universität Würzburg, Institut für Anorganische Chemie, Am Hubland, 97074 Würzburg, Germany

Supporting Information

ABSTRACT: In this work, we have explored for the first time the influence of conformational flexibility of π-core on chiral self-sorting properties of perylene bisimides (PBIs) that are currently one of the most prominent classes of functional dyes. For this purpose, two series of chiral macrocyclic PBIs **3a**−**c** and **4a**−**c** comprising oligoethylene glycol bridges of different lengths at the 1,7 bay positions were synthesized and their atropo-enantiomers (*P* and *M* enantiomers) were resolved. Single crystal analysis of atropo-enantiomerically pure (*P*)-**3a** not only confirmed the structural integrity of the ethylene glycol bridged macrocycle but also illustrated the formation of π-stacked dimers with left-handed supramolecular helicity. Our detailed studies with the series of highly soluble chiral PBIs **4a**−**c** by 1- and 2-D ^{1}H NMR techniques, and temperature- and concentration-dependent UV/vis absorption and circular dichroism (CD) spectroscopy revealed that in π−π-stacking dimerization of these PBIs chiral self-recognition (i.e., *PP* and *MM* homodimer formation) prevails over self-discrimination (i.e., *PM* heterodimer formation). Our studies clearly showed that with increasing conformational flexibility of PBI cores imparted by longer bridging units, the binding strength for the dimerization process increases, however, the efficiency for chiral self-recognition decreases. These results are rationalized in terms of an induced-fit mechanism facilitating more planarized π-scaffolds of PBIs containing longer bridging units upon π−π-stacking.

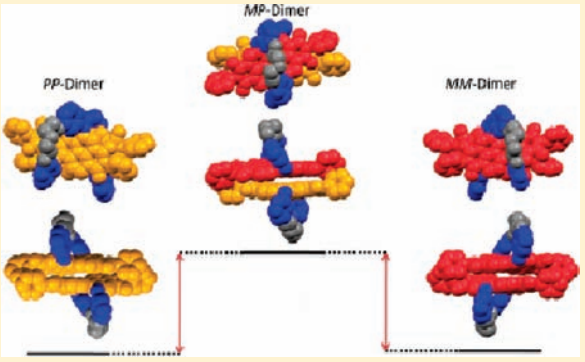

INTRODUCTION

Self-sorting[1] is an important branch of systems chemistry[2] that can be defined as high fidelity recognition of self, from nonself, between molecules in complex mixtures.[1a,e] Self-sorting can be classified as self-recognition if affinity for itself is shown, or self-discrimination if on the contrary affinity for others is observed.[1d] Chiral self-sorting is classified as well into self-recognition or self-discrimination,[3] depending on whether an enantiomer recognizes itself or its mirror image leading to the formation of homo- or heterochiral species, respectively. The importance of chiral self-sorting is evident, if we take into account the chiral nature of biomolecules such as sugars or aminoacids and the unknown origin of homochirality in life.[4] Studies on chiral self-sorting in perylene bisimide (PBI) dyes were recently started in our group with stable atropo-enantiomeric macrocyclic PBIs.[5] PBI dyes are an outstanding class of chromophores, which due to their optical and electronic properties[6] have been widely used for the development of functional organic materials.[7] Moreover, by means of X-ray diffraction analysis of different bay-substituted PBIs, it could be demonstrated that the introduction of substituents in the bay area leads to a twist of the two naphthalene units of the initial planar perylene core caused by repulsive interactions of these substituents.[8] Such contortion of the aromatic cores has been observed for other extended π-systems such as hexabenzocoronenes or helicenes.[9] The extent of this twisting is related to the bulkiness of the bay substituents varying from 4° for a 1,7-difluoro-substituted PBI[8a,8h] up to 37° for 1,6,7,12-tetrachloro derivatives.[8d,8f,10] A most interesting feature of the twisted perylene core is symmetry breaking leading to inherent chirality of the aromatic core. However, the isolation of single atropo-enantiomeric PBIs has been scarcely achieved as in most of the reported bay-substituted PBIs the two enantiomers are in a dynamic equilibrium.[11] To prevent racemization and, thus, to achieve configurationally stable atropo-enantiomeric and diastereomeric PBIs, our group has attached one or two bridging units shielding one or both of the PBI π-faces, respectively.[5,12] Similar approaches have been applied also for other dyes, for example,

Received: April 1, 2011
Published: May 09, 2011

dx.doi.org/10.1021/ja202696d | *J. Am. Chem. Soc.* 2011, 133, 9580–9591

Figure 1. Schematic representation of strapped atropo-enantiomeric PBIs and variation of the naphthalene units twisting angle depending on the bridge length.

porphyrins by Osuka and co-workers[13] and oligothiophenes by Takeuchi and co-workers,[14] or for some special liquid crystalline substances by Swager and co-workers[15] to induce intriguing mesophase properties. In a recent communication we have shown by NMR and concentration-dependent UV/vis studies the formation of $\pi-\pi$-stacked dimers with preferential self-recognition, that is, *MM* and *PP* dimers for a chiral PBI derivative with a rather short bridging unit connected to the 1 and 7 bay positions.[5] Other studies of self-sorting (chiral and general) of PBIs have been reported by Li and co-workers, however with conformationally unstable atropisomeric PBIs.[16a,b]

Here we present the synthesis of a series of chiral PBIs, bearing oligoethylene glycol (OEG) bridges of different lengths between the 1 and 7 bay positions. The substituents directly attached at the 1,7 positions are in all cases phenoxy units, which afford identical repulsive interactions between the bay substituents and, thus, an equal twist of the naphthalene entities derived thereof. However, elongation of the OEG bridging units provides the molecules with greater conformational flexibility, leading to less "imprinted" inherent chirality (see Figure 1), which profoundly affects two determinant features: chiral self-sorting of these molecules and binding strength in the dimerization process. We have observed that the increase of flexibility in the PBI cores adversely affects the self-recognition process. On the contrary, an increase of the binding strength by this dimerization process upon elongation of the bridging units has been observed, which revealed that induced-fit[17] plays a determinant role in our system. The induced-fit principle has been widely applied to explain the complexation process in various natural[17,18] and synthetic[19] host–guest systems, in which molecular flexibility allows undergoing structural changes to form more stable host–guest complexes or selective binding of specific guests. Quite similarly, our differently flexible macrocyclic PBIs undergo structural changes in order to form more stable self-assembled entities by optimizing the $\pi-\pi$-contact surfaces. These changes are more pronounced for the most flexible structures, a rather unprecedented feature in π-stacking dye aggregates.

EXPERIMENTAL SECTION

Cesium carbonate (99%) and potassium carbonate (≥99%) were obtained from commercial sources. All chemicals and reagents were used as received, unless otherwise stated. Potassium carbonate was dried *in vacuo* at 100 °C for 24 h. Diethylene glycol ditosylates were prepared according to literature procedures.[20] PBI derivatives **1** and **2** were prepared as previously reported.[5] Flash column chromatography was performed using silica gel (Si60, mesh size 40–63 μm). ^{1}H NMR spectra were recorded with Bruker Avance 400 MHz and Bruker DMX 600 MHz instruments. Chemical shifts are given in parts per million (ppm) and are referred to TMS as internal standard. ^{1}H coupling constants *J* are given in Hertz (Hz). Prior to ROESY measurement the samples were degassed with dry argon gas. Alternating-phase 180° pulses were applied during the mixing time in the ROESY experiments to suppress undesired TOCSY contributions.[21] High resolution mass spectra (HRMS) were recorded on a MicroTOF Focus from Bruker Daltonics. Analytical HPLC was carried out on a JASCO system (PU 2080 PLUS) with a diode array detector (MD 2015), equipped with a ternary gradient unit (DG-2080–533) and inline-degasser (LG 2080–02). Semipreparative HPLC was performed on a JASCO system (PU 2080 PLUS) with an UV/vis detector (UV 2077 PLUS). Preparative recycling GPC LC-9105, Japan Analytical Industry Co., Ltd. (JAI) was used in recycling mode for the resolution of some of the racemates. Vapor pressure osmometry (VPO) measurements were performed on a KNAUER osmometer with a universal temperature measurement unit. Benzil was used as standard and a calibration curve in terms of *R* (ohm) vs molal osmotic concentration (moles per kg *n*-hexane) was accomplished up to 0.016 *m*.

X-Ray Analysis. The crystal data of enantiopure (*P*)-**3a** were collected at a Bruker X8APEX diffractometer with CCD area detector and multilayer mirror monochromated MoK_α radiation. The structure was solved using direct methods and expanded applying Fourier techniques.[22] All non-hydrogen atoms were refined anisotropically. Hydrogen atoms were assigned to idealized positions and were included in structure factor calculations. For details see the Supporting Information and CCDC 818346.

UV/vis Absorption, Fluorescence, and Circular Dichroism (CD) Spectroscopy. For all spectroscopic measurements, spectroscopic grade solvents (Uvasol) from Merck were used. UV/vis spectra were recorded with a Perkin-Elmer Lambda 950 spectrometer equipped with a PTP-1 peltier element. CD spectra were measured with a JASCO J-810 spectrometer equipped with a CDF-242 peltier element. Fluorescence spectra were recorded with a PTI QM-4/2003 instrument. All fluorescence measurements were performed at room temperature and fluorescence spectra were corrected against photomultiplier and lamp intensity. The fluorescence quantum yields were determined as the average value for three different excitation wavelengths using *N*,*N*′-di(2,6-diisopropylphenyl)-3,4:9,10-tetracarboxylic acid bisimide as reference (Φ_{fl} = 100% in chloroform) by applying high dilution conditions ($A < 0.05$).[23] For the measurements at high concentrations, front-face set up with 30° light beam angle deviation and 1 mm cells were used. Fluorescence lifetimes were measured under ambient conditions by using a PTI LaserStrobe fluorescence lifetime spectrometer system containing a GL-3300 nitrogen laser (337.1 nm, pulse width 600 ps, pulse energy 1.45 mJ) coupled with a dye laser GL-302 (pulse width 500 ps, pulse energy 220 μJ at 550 nm) as an excitation source and a stroboscopic detector. Laser output was tuned within the emission curves of the laser dyes supplied with the instrument (PLD 421, 500, 579, 665, 735). The time resolution following deconvolution of experimental decays is 200 ps. The instrument response function was collected by scattering the exciting light of a dilute, aqueous suspension of Silica (LUDOX). Decay curves were evaluated using the software supplied with the instrument applying least-squares regression analysis. The quality of the fit was evaluated by analysis of χ^2 (0.9 – 1.1), DW factor (>1.75) and *Z* value (<−1.96, confidence level 0.95) as well as by inspection of residuals and autocorrelation function.

Computational Details. Ground-state DFT structure optimizations for **4a** have been done with the Turbomole program package (version 5.9.1)[24] at the RI-BLYP-D/TZV(P) level[25] including the empirical dispersion corrections by Grimme et al.[26] The same method has recently been shown to provide accurate structures and binding energies for unbridged PBI dimers.[27] The $C_{12}H_{25}$ chains in **4a** were simplified to hydrogen atoms for computational efficiency.

Synthesis of PBIs 3b,c. *N*,*N*′-Dicyclohexyl-1,7-(3-hydroxyphenoxy)perylene-3,4:9,10-tetracarboxylic acid bisimide **1**[5] (230 mg, 0.30 mmol for **3b** and 400 mg, 0.52 mmol for **3c**) and cesium carbonate

(1.7 g, 5.21 mmol for **3b** and 3 g, 9.20 mmol for **3c**) were dissolved in DMSO (150 mL for **3b** and 500 mL for **3c**) and heated to 120 °C for 7 h. The addition of the respective tri or tetra(ethylene glycol) distosylate (280 mg, 0.57 mmol and 520 mg, 1.00 mmol, respectively) dissolved in DMSO (20 mL) was carried out with a syringe pump over a period of 3 h. The reaction mixture was cooled to ambient temperature and dropped into 0.33 M hydrochloric acid (150 mL) under stirring. The resulting precipitate was collected by filtration and dried *in vacuo* (10 mbar). Column chromatography with silica gel and dichloromethane (DCM) for **3b** and alox (neutral) and DCM for **3c**, with subsequent precipitation with methanol from DCM solution afforded 61.0 mg (0.069 mmol) of **3b** (23% yield) as an orange solid and 74.2 mg (0.078 mmol) of **3c** (15% yield) as a red solid.

3b. Mp 318−319 °C. ^{1}H NMR ($CDCl_3$): δ 9.42 (d, 2H, J = 8.2), 8.55 (d, 2H, J = 8.2), 8.38 (s, 2H), 7.32 (t, 2H, J = 8.3), 7.10 (m, 2H), 6.48 (m, 2H), 5.80 (s, 2H), 5.00 (m, 2H), 3.82−3.73 (m, 4H), 3.63−3.42 (m, 8H), 2.53 (m, 4H), 1.89 (bd, 4H), 1.74 (bd, 6H), 1.53−1.25 (m, 6H). HRMS (ESI-TOF, pos. mode, DCM/acetonitrile = 1:1): m/z calc. for $C_{54}H_{49}N_2O_{10}$ $[M + H]^+$: 885.3309, found: 885.3382. UV/vis (DCM): λ_{max}/nm (ε_{max}/$M^{-1}cm^{-1}$) 522 (64 000), 486 (39 900), 454 (14 800), 266 (33 200). Fluorescence (DCM): λ_{max} = 532 nm (λ_{ex} = 525 nm), Φ_{fl} = 0.33.

3c. Mp 210−211 °C. ^{1}H NMR ($CDCl_3$): δ 9. 53 (d, 2H, J = 8.5), 8.58 (d, 2H, J = 8.5), 8.34 (s, 2H), 7.38 (t, 2H, J = 8.2), 7.11 (m, 2H), 6.63 (m, 2H), 6.03 (t, J = 2.3, 2H), 5.00 (m, 2H), 3.88−3.78 (m, 4H), 3.65−3.61 (m, 4H), 3.51−3.44 (m, 8H), 2.53 (m, 4H), 1.89 (bd, 4H), 1.74 (bd, 6H), 1.53−1.25 (m, 6H). HRMS (ESI-TOF, pos. mode, DCM/acetonitrile =1:1): m/z calc. for $C_{56}H_{52}N_2O_{11}Na$ $[M + Na]^+$: 951.3469, found: 951.3463, λ_{max}/nm (ε_{max}/M^{-1} cm^{-1}) 525 (55 800), 488 (35 500), 458 (13 800), 265 (35 200). Fluorescence (DCM): λ_{max} = 551 nm (λ_{ex} = 525 nm), Φ_{fl} = 0.57.

Resolution of *P*-(+)-3 and *M*-(−)-3 Enantiomers by HPLC. Separation of the enantiomers was achieved on a semipreparative column (Trentec Reprosil 100 chiral-NR) using different mixtures of *n*-hexane and DCM as eluent.

3b was eluted in a 3/2 mixture of DCM/ *n*-hexane using a flow of 8 mL/min. The separation was done on a scale of 15 mg.

M-(−)-**3b**: Retention time (Trentec Reprosil 100 chiral-NR, DCM/*n*-hexane (3/2), flow: 8.0 mL min^{-1}; Ø = 2.5 cm): 22.0 min. CD (DCM): λ_{max}/nm ($\Delta\varepsilon$/M^{-1} cm^{-1}): 518 (−47), 484 (−31), 454 (−12), 286 (−86), 262 (+64).

P-(+)-**3b**: Retention time (Trentec Reprosil 100 chiral-NR, DCM/*n*-hexane (3/2), flow: 8.0 mL min^{-1}; Ø = 2.5 cm): 32.0 min. CD (DCM): λ_{max}/nm ($\Delta\varepsilon$/M^{-1} cm^{-1}): 518 (+44), 484 (+30), 454 (+11), 286 (+86), 262 (−64).

3c was eluted in a 4/1 mixture of DCM/*n*-hexane using a flow of 8 mL/min. The separation was done on a scale of 15 mg.

M-(−)-**3c**: Retention time (Trentec Reprosil 100 chiral-NR, DCM/*n*-hexane (4/1), flow: 8.0 mL min^{-1}; Ø = 2.5 cm): 10.0 min. CD (DCM): λ_{max}/nm ($\Delta\varepsilon$/M^{-1} cm^{-1}) 522 (−34), 486 (−23), 458 (−9), 287 (−59), 264 (+36).

P-(+)-**3c**: Retention time (Trentec Reprosil 100 chiral-NR, DCM / *n*-hexane (4/1), flow: 8.0 mL min^{-1}; Ø = 2.5 cm): 12.0 min. CD (DCM): λ_{max}/nm ($\Delta\varepsilon$/M^{-1} cm^{-1}) 522 (+37), 486 (+24), 458 (+9), 287 (+47), 264 (−39).

Synthesis of PBIs 4b,c. *N*,*N*′-Di(3,4,5-tridodecylphenyl)-1,7-di(3-hydroxyphenoxy)perylene-3,4:9,10- tetracarboxylic acid bisimide **2**[5] (300 mg, 0.17 mmol for both **4b** and **4c**), and cesium carbonate (1 g, 3.06 mmol) were dissolved in dry THF (400 mL) and refluxed at 90 °C for 7 h. The addition of the correspondent tri or tetra(ethylene glycol) distosylate (150 mg, 0.31 mmol and 170 mg, 0.32 mmol, for **4b** and **4c** respectively) dissolved in THF (20 mL) was carried out with a syringe pump over a period of 6 h. The reaction mixture was cooled to ambient temperature and dropped into 0.33 M hydrochloric acid (150 mL) under stirring. The resulting precipitate was collected by filtration and dried *in vacuo* (10 mbar). Silica gel (**4b**: DCM /*n*-hexane, 1/1; **4c**: DCM/*n*-hexane, 3/2) column chromatography and precipitation with methanol from DCM solution afforded 146 mg (0.078 mmol) of **4b** (22% yield) and 50.1 mg (0.026 mmol) of **4c** (15% yield) as an orange solid.

4b. Mp 180−190 °C. ^{1}H NMR ($CDCl_3$): δ 9.52 (d, 2H, J = 8.2), 8.64 (d, 2H, J = 8.2), 8.48 (s, 2H), 7.33 (t, 2H, J = 8.3), 7.10 (m, 2H), 6.93 (m, 2H), 6.50 (s, 2H), 5.87 (m, 2H), 3.90−3.62 (m, 4H), 3.55−3.48 (m, 8H), 2.64 (t, 12H, J = 7.8), 1.59−1.55 (m, 12H), 1.32−1.18 (m, 108H), 0.83−0.78 (m, 18H). HRMS (ESI-TOF, pos. mode, DCM/acetonitrile = 1:1): m/z calc. for $C_{126}H_{181}N_2O_{10}$ $[M + H]^+$: 1882.3716, found: 1882.3711. UV/vis (DCM): λ_{max}/nm (ε_{max}/M^{-1} cm^{-1}) 524 (77 700), 488 (48 100), 457 (18 100), 263 (43 000). Fluorescence (DCM): λ_{max} = 534 nm (λ_{ex} = 525 nm), Φ_{fl} = 0.14.

4c. Mp 148 °C−155 °C. ^{1}H NMR ($CDCl_3$): δ 9.62 (d, 2H, J = 8.3), 8.67 (d, 2H, J = 8.3), 8.44 (s, 2H), 7.37 (t, 2H, J = 8.2), 7.11 (m, 2H), 6.93 (m, 2H), 6.03 (t, J = 2.3, 2H), 6.10 (m, 2H), 3.92−3.82 (m, 4H), 3.67−3.65 (m, 4H), 3.55−3.48 (m, 8H), 2.63 (t, 12H, J = 8.0), 1.59−1.55 (m, 12H), 1.32−1.18 (m, 108H), 0.83−0.78 (m, 18H). HRMS (ESI-TOF, pos. mode, DCM/acetonitrile = 1:1): m/z calc. for $C_{127}H_{182}N_2O_{11}$ $[M + H]^+$: 1926.39001, found: 1926.39729, λ_{max}/nm (ε_{max}/M^{-1} cm^{-1}) 526 (64 900), 491 (41 300), 461 (15 800), 263 (43 000). Fluorescence (DCM): λ_{max} = 551 nm (λ_{ex} = 525 nm), Φ_{fl} = 0.25.

Resolution of *P*-(+)-4 and *M*-(−)-4 Enantiomers by HPLC. Separation of the enantiomers was achieved on a semipreparative column (Trentec Reprosil 100 chiral-NR) using different mixtures of *n*-hexane and chloroform.

4b. **4b** was eluted in a 65/35 mixture of chloroform/*n*-hexane using a flow of 3.5 mL min^{-1}. The separation was done in the JAI recycling system, after 7 cycles and two iterations on a scale of 10 mg.

M-(−)-**4b**: CD (DCM): λ_{max}/nm ($\Delta\varepsilon$/M^{-1} cm^{-1}): 522 (−43), 487 (−30), 456 (−12), 286 (+69), 263 (−67).

P-(+)-**4b**: CD (DCM): λ_{max}/nm ($\Delta\varepsilon$/M^{-1} cm^{-1}): 522 (+45), 487 (+30), 456 (+12), 286 (−69), 263 (+69).

4c. **4c** was eluted in a 7/3 mixture of chloroform/*n*-hexane using a flow of 10 mL min^{-1}. The separation was done in the JAI recycling system, after 7 cycles and five iterations on a scale of 5 mg.

M-(−)-**4c**: CD (DCM): λ_{max}/nm ($\Delta\varepsilon$/M^{-1} cm^{-1}): 525 (−33), 488 (−18), 456 (−7), 286 (+ 32), 263 (−37).

P-(+)-**4c**: CD (DCM): λ_{max}/nm ($\Delta\varepsilon$/M^{-1} cm^{-1}): 525 (+37), 488 (+24), 456 (+11), 286 (− 39), 263 (+37).

RESULTS

Synthesis. PBIs **3** and **4** were synthesized from previously reported[5] precursors **1** and **2**, respectively (Scheme 1). The 3,4,5-trisdodecylphenyl substituents in PBIs **4a**−**c** were introduced to provide the molecules with improved solubility properties, while the cyclohexane substituents in PBIs **3a**−**c** facilitate the single crystal growth. The free OH groups of PBIs **1** and **2** are available for a two-fold Williamson etherification with differently sized ditosylates.[28] The macrocyclization reaction takes place in the presence of cesium carbonate, which is known to facilitate ring closures.[29] A solution of the respective ditosylate was slowly dropped over several hours by using a syringe pump into a solution of the precursors **1** or **2** in DMSO or THF, respectively. After work up of the reaction mixtures, the desired macrocycles **3a**−**c** and **4a**−**c** could be isolated as racemates. The chiral resolution of these PBIs could be achieved by HPLC on a chiral column (Trentec Reprosil 100 chiral-NR) using different experimental conditions for each macrocycle in a purity of over 99%.

Optical Properties of the Monomers. The optical properties of monomeric macrocycles **3** and **4** were investigated by UV/vis,

Scheme 1. Synthetic Route and Chiral Resolution of Macrocyclic PBIs 3 and 4

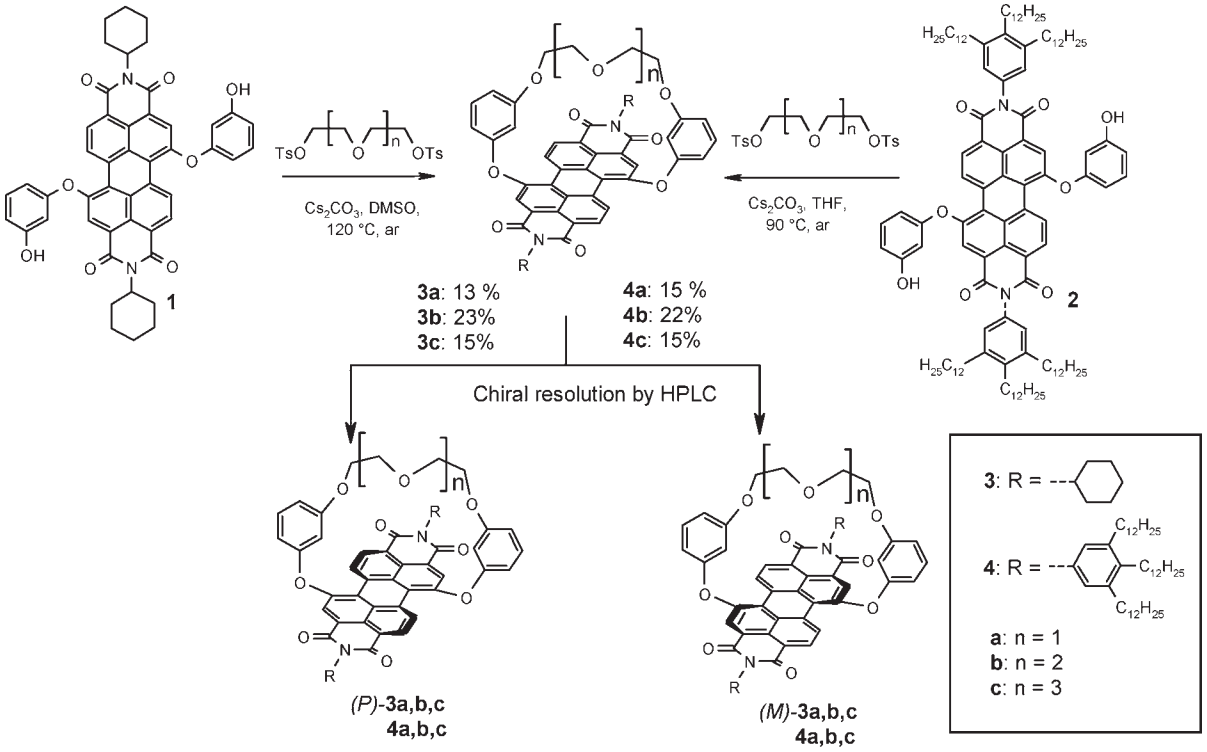

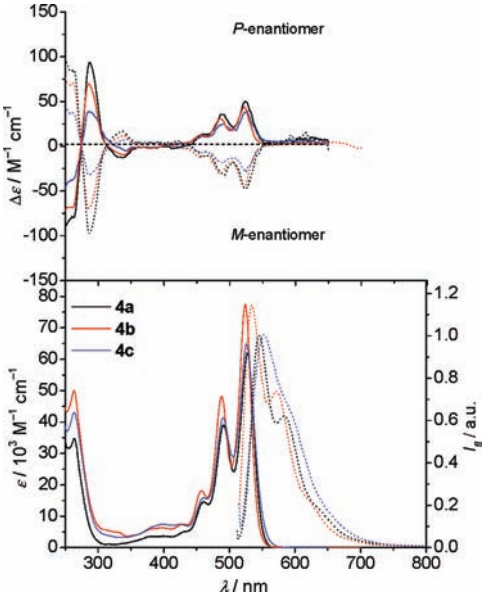

Figure 2. (Bottom) UV/vis absorption spectra (solid lines) of racemic PBIs **4a**−**c** in DCM at 5×10^{-6} M and normalized emission fluorescence spectra ($\sim 10^{-7}$ M, dashed lines, λ_{ex} = 525 nm) in DCM of **4a**−**c**: **4a** (black line), **4b** (red line) and **4c** (blue line) at RT. (Top) CD spectra of *P* enantiomer (solid lines) and *M* enantiomers (dashed lines) of **4a**−**c** in DCM at 5×10^{-6} M at RT.

fluorescence and circular dichroism (CD) spectroscopy. The UV/vis absorption of the racemates (no changes are observed in comparison with the UV/vis spectra of their enantiomers) and CD spectra of their respective enantiomers in dichloromethane (DCM) are shown in Figure 2 and Figure S1 in the Supporting Information, and their optical data are summarized in Tables 1 and 2. The absorption spectra of macrocyclic PBIs **3a**−**c** and **4a**−**c** reveal S_0−S_1 transition with three vibronic progressions between 527−524 nm, 492−490 nm and 462−459 nm in DCM (Figures 2 and S1 in the Supporting Information). The higher energetic S_0−S_2 transition has diminished in the case of **3a** and **4a**, while for **3c** and **4c** it is clearly visible. The absorption coefficients are lower for **3a**−**c** derivatives than for the respective derivatives **4a**−**c** (Table 1 and 2). This appears to be a general absorption phenomenon and has been observed for other PBIs with alkyl or aryl substituents in imide positions.[30] Some minor changes in the shape of the UV/vis spectra are observed for **3a**/**4a**, **3b**/**4b** and **3c**/**4c** that should be attributed to structural changes related to the different bridge lengths. The CD spectra of *M* and *P* enantiomers of **3a**−**c** and **4a**−**c** (top panels, Figure 2 and S1 in the Supporting Information) are mirror images as expected for pure enantiomers. The stereochemical assignment of these enantiomers was achieved by comparison of the respective CD spectra with those of previously reported structurally similar epimerically pure *P*- and *M*-configured macrocyclic PBIs.[31]

Bisignate Cotton effects are not observed in the visible region. This observation and the absence of further transitions in excitonic coupled states in the spectral region of the monomer S_0−S_1 absorption support the exclusive presence of monomeric species at this concentration ($c = 5 \times 10^{-6}$ M) in DCM. The fact that the CD signal decreases in intensity upon increasing the bridge length (top panels, Figure 2, Table 1 and 2) provides further evidence that this CD band solely originates from the

dx.doi.org/10.1021/ja202696d |*J. Am. Chem. Soc.* 2011, 133, 9580–9591

Table 1. Optical Properties of Macrocyclic PBIs 3a−c in DCM at RT

	$\lambda_{max(abs)}$/ nm	ε/ $M^{-1}\,cm^{-1}$	$\lambda_{max(em)}$/ nm	Φ_{fl}/ %	$\Delta\varepsilon\ (P)^a$/ $M^{-1}\,cm^{-1}$	$\Delta\varepsilon\ (M)^a$/ $M^{-1}\,cm^{-1}$
3a	525	56 000	538	27	51	−49
3b	522	64 000	533	33	43	−44
3c	525	56 000	550	57	36	−33

[a] Determined for maximum emission of S_0-S_1 transition.

Table 2. Optical Properties of Macrocyclic PBIs 4a−c in DCM at RT

	$\lambda_{max(abs)}$/ nm	ε/ $M^{-1}\,cm^{-1}$	$\lambda_{max(em)}$/ nm	Φ_{fl}/ %	$\Delta\varepsilon\ (P)^a$/ $M^{-1}\,cm^{-1}$	$\Delta\varepsilon\ (M)^a$/ $M^{-1}\,cm^{-1}$
4a	525	65 000	545	9	49	−47
4b	522	76 000	534	14	43	−45
4c	525	65 000	553	25	37	−33

[a] Determined for maximum emission of S_0-S_1 transition.

twisted core. The drop of the signal intensity is about 33% from **3a**,**4a** (shortest bridge) to **3c**,**4c** (largest bridge) in the visible region. The latter effect is even more pronounced in the ultraviolet region with a descent in the intensity of about 58%. Here, a distinct bisignate Cotton effect is observed that can be attributed to the chiral excitonic coupling between transition dipole moments that are polarized perpendicular to the long molecular axis within the two naphthalene subunits in the PBI aromatic core. The magnitude of $\Delta\varepsilon$ for such excitonic coupling is directly related to the twist angle, which is a consequence of repulsive interactions between the sterically encumbered bay substituents.[8d−f,12a] Although racemization via interconversion of atropo-enantiomers is not possible for PBIs **3** and **4** due to the bridging unit on one π-surface, the decrease of the intensity of the CD signal especially in this ultraviolet region is a clear indication that on average a less pronounced twisting angle is adopted upon increasing the bridge length, pointing to partial planarization or even temporary flip of the naphthalene units as suggested in Figure 1 for the most flexible PBIs **3c** and **4c**. For these two macrocyclic PBIs with the longest OEG chains, a partial interconversion between *M* and *P* forms can be imagined based on molecular modeling studies. However, on average the chiral sense is preserved as evidenced by the sign of the CD spectra. Therefore, all these macrocyclic PBIs can be considered as configurationally stable chiral molecules.

The fluorescence spectra of **3** and **4** show similar progressions as their UV/vis spectra, however, are less pronounced upon increasing bridge length. The observed emission maxima are between 532 and 553 nm (Figure 2 and S2 in the Supporting Information). The emission maxima at the longest wavelengths are concomitant with the largest Stokes shifts observed for **3c** and **4c**, suggesting more pronounced structural relaxation processes of these more flexible molecules in the excited state. Similarly large or even larger Stokes shifts have been observed for tetraphenoxy-substituted PBIs that were attributed to pronounced reorientation of those substituents.[32] Again, no significant spectral differences are found for the racemic mixtures and their respective pure enantiomers. The fluorescence quantum yields have been determined in DCM (Table 1 and 2) using *N*,*N*′-di(2,6-diisopropylphenyl)-3,4:9,10-tetracarboxylic acid bisimide as reference (Φ_{fl} = 100% in $CHCl_3$). It can be noticed that the quantum yield increases upon enlarging the bridging unit. This phenomenon has been observed previously and explained for double-bridged PBIs.[12a]

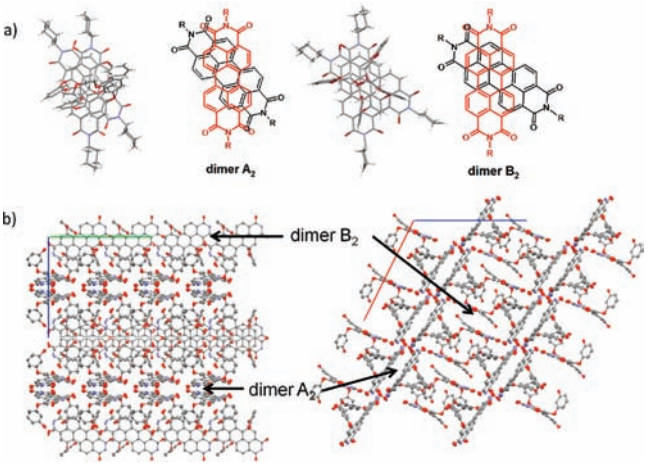

Figure 3. (a) $\pi-\pi$ interaction between two PBI molecules in a dimer observed in the solid state structure of (*P*)-**3a**: Crystal packing (left) and corresponding structural representation (right) of dimer A_2 and dimer B_2. In the structural representation, the top molecule is highlighted in red and the substituents in the bay area were omitted for clarity. (b) Molecular packing of (*P*)-**3a** in the solid state. View along the *a*-axis (left) and *b*-axis (right). The red line represents the *a*-axis, the green line the *b*-axis, and the blue line the *c*-axis of the unit cell. Di(ethylene glycol) bridges and included solvent molecules are omitted for clarity.

X-Ray Diffraction Analysis. Single crystals of enantiopure (*P*)-**3a** suitable for X-ray diffraction were obtained by dissolving this compound in dichloromethane and addition of equal amounts of methanol, followed by slow evaporation of the solvent. The enantiomerically pure (*P*)-**3a** crystallized in the monoclinic space group C_2 and two crystallographically independent molecules were found in the unit cell (Figure 3a).

The torsion of the central six-member ring was determined for one type of molecules (denoted as B) to 16.9° and 18.5°, and for the other (denoted as A) to 16.8° and 9.8°. Molecule A possesses a bowl-like structure whereas the second type of molecule (B) does not show any distortion along the *N*,*N*-axis of the perylene bisimide. The low torsion of 9.8° as well as the bowl-like bending of A might be due to packing effects. Even more interesting than the molecular structures of A and B is the solid state packing of the enantiopure macrocycle (*P*)-**3a**, as exclusive formation of π-dimers for these homochiral macrocycles is observed, providing interesting structural information about the supramolecular arrangement. The dimers are arranged in two perpendicular layers with the perylene plane of **3a** being either perpendicular to the *a*-axis (dimer B_2) or the *c*-axis (dimer A_2) of the unit cell (Figure 3b). The closest distance between the molecules was determined to 3.27 Å for dimer B_2 whereas for both π-dimers the mean distance between two perylene bisimide π-surfaces was elucidated to 3.47 Å (see Figure S4 in the Supporting Information), which matches well with the distance observed in the solid state for the $\pi-\pi$ interactions (3.34−3.55 Å) of the fully planar core-unsubstituted PBIs.[33] Both dimers A_2 and B_2 are characterized by a rotational offset of 43° and 58°, respectively. The rotational offset is accompanied by a longitudinal offset along the *N*,*N*-axis of the perylene bisimide which is negligible for dimer A_2 but pronounced for dimer B_2. The helicity of the dimers induced by the rotational offset can be

dx.doi.org/10.1021/ja202696d | *J. Am. Chem. Soc.* 2011, 133, 9580–9591

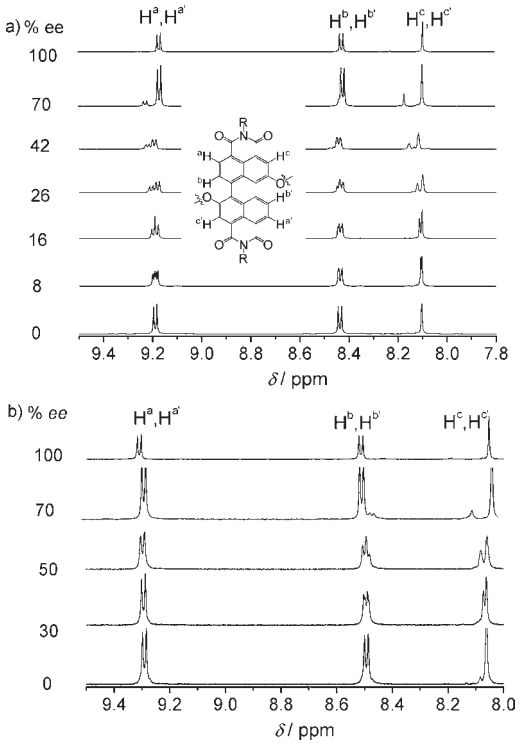

Figure 4. 600 MHz ^{1}H NMR spectra of solutions with different *ee* in *n*-hexane-d_{14} at 331 K ($c = 2 \times 10^{-3}$ M) (range of PBI protons) for (a) **4b** and (b) **4c**.

assigned as left-handed for both dimers A_2 and B_2. This indicates that the (*P*)-configuration of the twisted perylene core enforces the formation of dimers with left-handed supramolecular chirality. In contrast to enantiopure (*P*)-**3a**, no π-stacked dimers could be observed in single crystals of racemic PBI **3a**.[5] Attempts to grow single crystals of PBIs **3b** and **3c** using the same procedure as applied for PBI **3a** were not successful, probably due to the more flexible bridging units of the former structures.

Dimer Formation in Solution. Dimer formation of highly concentrated solutions of **4a**−**4c** could be demonstrated by vapor pressure osmometry (VPO) measurements. VPO experiments of **4b** and **4c** ($c = 1 \times 10^{-3}$ to 5×10^{-3} M) in *n*-hexane at 328 K using benzil for calibration gave aggregation numbers *N* ($N = K_{cal}/K_{mean}$) of 1.81 and 2.05, respectively (Figure S5 in the Supporting Information).

Comparative ^{1}H NMR studies of **4b**,**c** (racemates and their respective pure enantiomers) in *n*-hexane-d_{14} at 331 K were performed to elucidate structural differences between homo- and heterochiral dimers. At the measured concentration, dimers are the major species as indicated by VPO and concentration-dependent UV/vis studies (about 80 and 90% of dimers are present in **4b** and **4c**, respectively, according to the data shown in Figures 8 and S7b−S12b in the Supporting Information). In contrast to the spectra measured at room temperature (RT), the ^{1}H NMR signals obtained at 331 K are sharper, thus allowing a quantitative evaluation of the NMR data. The superposed spectra of the racemates and their respective enantiomers revealed some differences in the shift of the aromatic protons, especially the ones corresponding to the protons of the PBI core. We have previously demonstrated that the observed differences between the racemates and their respective pure enantiomers are related to the contemporaneous presence of homo and heterochiral dimers in the racemic solution.[5] For macrocycle **4a** it was found that for solutions with % *ee* not equaling 0 or 100% at $c = 2 \times 10^{-3}$ M two sets of signals appear for each PBI core proton pair (H^a,$H^{a'}$, H^b, $H^{b'}$, and H^c,$H^{c'}$, see Figure 4). The signal splitting of these protons is related to the different chemical environments of H^x and $H^{x'}$ (x = a, b, or c) when they are in a homodimer or in a heterodimer, or what is the same, due to the diastereomeric relationship between homo- and heterodimers. The relative intensities of the two signals related to one proton (H^x $H^{x'}$) of **4a** correspond to the enantiomeric ratio, which can be directly related to the % *ee*, and thus the integration of the NMR signals can be used as direct measure of the % *ee*. Such correlation of the intensities of NMR signals and the *ee* indicates that the system is under fast exchange conditions.[34] Similarly, splitting of the signals at % *ee* different from 0 and 100% was found for **4b** and **4c**, pointing to diastereomeric relationships of the dimers (homo and heterochiral) present in solution (Figure 4). However, for **4b** the splitting of the signals is less pronounced than for **4a**, and the splitting of **4c** is even less pronounced than for **4b** (Figure 4). This phenomenon indicates that upon increasing the bridge length and hence the flexibility of the molecules, the diastereomeric relationship between the homo and heterochiral dimers becomes less evident.

Consequently, the observed splitting of NMR signals is also less pronounced for the macrocyclic PBIs with larger bridging units (**4b** and **4c**), which prohibits a proper analysis of the data over the entire concentration range. Nevertheless, at least for **4b**, the % *ee* can be determined from H^c,$H^{c'}$ signals between 100 and 26% (Table S1 in the Supporting Information).

ROESY and COSY NMR Spectroscopy. Several attempts were made to obtain proper ROESY spectra of macrocycles (*P*)-**4a**−**c** (or (*M*)-**4a**−**c**) at 331 and 298 K in *n*-hexane-d_{14} at a concentration of 2×10^{-3} M. The advantage of the measurements at high temperature (331 K) is the sharpening of the NMR signals. Unfortunately, no intermolecular cross peaks at this temperature could be observed in any of the ROESY experiments performed for these pure enantiomeric PBIs. We attribute this fact to the fast exchange conditions at this temperature. To overcome this drawback, experiments at 298 K were performed with (*P*)-**4a**−**c**. At this temperature, the NMR signals of macrocyclic (*P*)-**4a** and (*P*)-**4c** are too broad, especially in the aromatic region for ROESY measurements. Fortunately, for (*P*)-**4b** signals, which are sharp enough for recording, a successful ROESY spectrum was found at RT (Figure 5a).

As expected, intramolecular cross peaks between neighboring aromatic protons H^a and H^b can be observed in the ROESY spectrum. More interestingly, a much weaker cross peak appears between the distant aromatic protons H^a and H^c (Figure 5a). To rule out the possibility that this cross peak originates from the indirect coupling between H^a and H^c protons through the aromatic naphthalene unit, a COSY experiment was carried out under the same conditions as for the ROESY one. As can be appreciated in Figure 5b, expected intramolecular cross peaks between aromatic protons H^a and H^b can be observed. However, no trace of the cross peak resulting from the coupling between aromatic protons H^a and H^c is present. Accordingly, this cross peak between H^a and H^c is attributed to an intermolecular contact in the homochiral dimer where these protons come into close proximity (see DFT calculations also).[35]

Optical Properties of the Dimers. The aggregation behavior of PBIs **4a**−**c** (racemate and pure enantiomers) was investigated

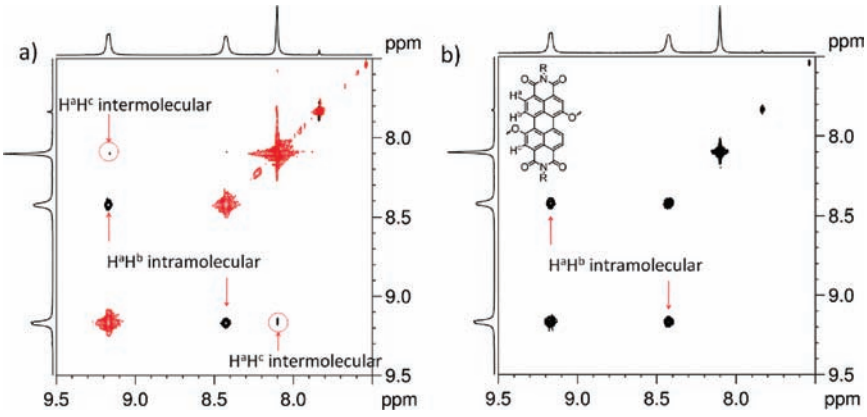

Figure 5. 600 MHz (a) ROESY and (b) COSY NMR data of (*P*)-**4b** in *n*-hexane-d_{14} at 298 K ($c = 2 \times 10^{-3}$ M) (range of PBI protons). The ROESY spectrum was recorded with a mixing time of 200 ms. Positive and negative signals are represented by black and red lines, respectively.

by concentration-dependent UV/vis, CD and fluorescence spectroscopy in a concentration range between 10^{-6} and 10^{-3} M in *n*-hexane (for CD and fluorescence) and *n*-heptane (for UV/vis) at RT.[36]

Concentration-dependent UV/vis studies of **4a**−**c** in *n*-heptane show pronounced spectral changes, including a hypsochromic shift of the absorption maxima upon increasing concentration (Figure 6, bottom panels), indicating the formation of H-type aggregated species.[37] Concentration-dependent UV/vis spectra show no evident differences between racemates and pure enantiomers (Figures 6 and S7−S12 in the Supporting Information). Spectral changes, however, are observed in the shape of the absorption bands for differently bridged PBIs **4a**−**c**, being most pronounced for the aggregate spectrum of **4c** (Figure 6c). Two clear isosbestic points are observed at about 470 and 525 nm (more or less shifted for **4a**, **4b** or **4c**), confirming the presence of two species, that is, monomeric and dimeric, in equilibrium. CD spectra of **4a**−**c** *M* and *P* enantiomers were measured at concentration of 1×10^{-3} (strongly aggregated) and 5×10^{-6} M (not aggregated) in *n*-hexane at RT (see Figure 6, top panels). Hypsochromic shifts of the CD maxima are observed in accordance with the spectral changes recorded in the UV/vis spectra. Characteristic bisignate Cotton signals are present for all studied macrocyclic PBIs, indicating the helical nature of the formed dimers in solution, as it has been previously demonstrated for PBI **4a**.[5] The negative sign of the exciton couplet for (*P*)-**4a**−**c** points to a left-handed helicity (the opposite for (*M*)-**4a**−**c**) of the respective dimeric aggregate according to exciton chirality method.[38] Interestingly, the intensity of the bisignate signal in the ultraviolet region corresponding to the chiral exciton coupling between the transition localized in the two naphthalene subunits of the PBI core is reduced in the case of the dimeric aggregates compared to the respective monomeric dyes **4a**−**c**. This result can be attributed to a decrease of the core twisting angle of these macrocyclic PBIs upon $\pi-\pi$-stacking after optimization of the contact surfaces of the interacting naphthalene subunits, and thus a special case of "induced-fit" mechanism can be implicated for the π-stacking dimerization of PBIs **4a**−**c**.

Concentration-dependent fluorescence spectra of **4a**−**c** are shown in Figures 7 and S6 in the Supporting Information. The most remarkable feature is that fluorescence spectra of highly concentrated solutions ($c = 5 \times 10^{-4}$ M) show similar excimer-type emission as observed for extended π-stacks.[37,39] The pronounced concentration dependence indicates that these excimers are not formed from excited monomeric PBIs by diffusion but originated from photoexcited PBI dimers.

To further elucidate the fluorescence properties of these macrocyclic PBIs **4a**−**c** lifetime experiments were carried out. The fluorescence decay times monitored at the monomer band (535 nm) and the aggregate band (610 nm) are collected in Table S2 in the Supporting Information. Lifetime decay values of about 4 and 32 ns for the monomer and dimer bands, respectively, were found in all cases, in good accordance with values found for extended self-assembled π-stacks of PBIs[40] and covalently fixed dimeric π-stacks.[41] It is remarkable, that neither the shape of the fluorescence spectra nor the fluorescence decay values are strongly affected by the length of the bridge unit in **4a**−**c** which is in striking contrast to UV/vis and CD spectra. The rationale behind these differences might be that the dimer aggregates of these PBIs exhibit more similar structures in the relaxed excited state than in the ground state. Quantum chemical calculations have suggested a structural rearrangement of PBI dimers in the excimer state,[27] which might indeed afford quite similar structures for all three PBI derivatives.

DISCUSSION

Quantification of Chiral Self-Sorting and Effect of Temperature. The binding constants K_D for the dimerization of (*rac*)-**4a**−**c**, (*P*)-**4a**−**c** and (*M*)-**4a**−**c** were determined by concentration-dependent UV/vis spectroscopy at 331 K (Figure 8 and S7−S12 in the Supporting Information and ref 5) in *n*-heptane.

The concentration-dependent UV/vis absorption spectra of the racemates and their respective pure enantiomers (all experiments were repeated twice) of these three macrocyclic compounds appear virtually identical, indicating similar aggregation behavior. The fitting of the experimental data obtained from the concentration-dependent UV/vis absorption studies can be carried out by nonlinear regression analysis using the dimerization model[42] or applying a multilinear analysis of the data carried out by a custom-made program.[43] Preferential self-recognition, that is, formation of homo dimers, at 331 K in *n*-heptane could recently be proven for compound **4a** with such methods.[5] Thus, similar studies on **4b** and **4c** will provide enough information to unravel the influence of the increasing molecular flexibility of the PBI derivatives on their chiral self-sorting. Moreover, all measurements were repeated at 298 K (see Figures S13−S21 in the

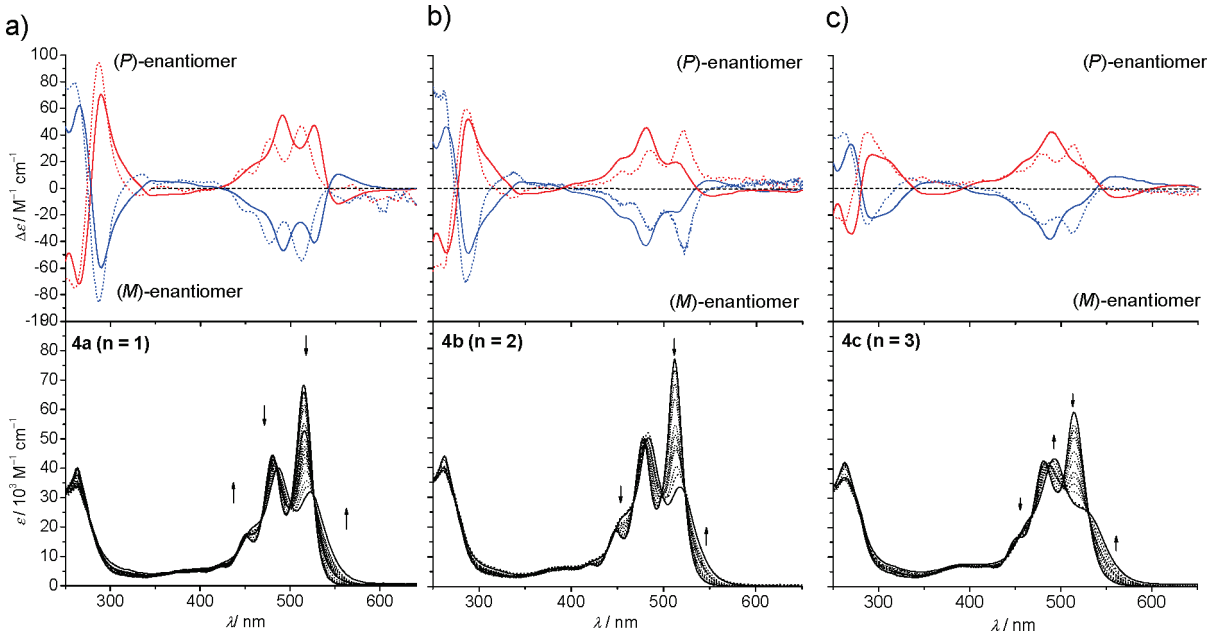

Figure 6. Concentration-dependent UV/vis absorption (racemates, bottom panels) in *n*-heptane and CD spectra (enantiomers, top panels; (*M*)-enantiomer: blue lines, (*P*)-enantiomer: red lines) of **4a**−**c** in *n*-hexane, in the range from 5×10^{-6} M (dashed lines) to 1×10^{-3} M (solid lines) at RT for (a) **4a**, (b) **4b**, and (c) **4c**. Arrows indicate changes upon increasing concentration.

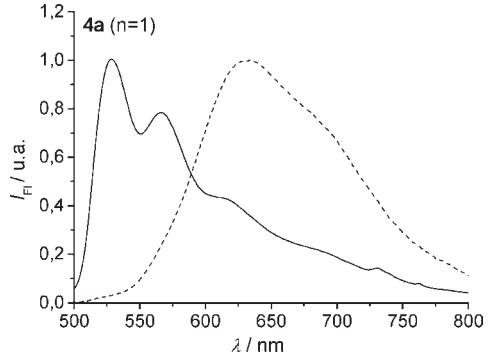

Figure 7. Normalized concentration-dependent fluorescence spectra of **4a** in *n*-hexane at 5×10^{-4} M (dashed line) to 5×10^{-6} M (solid line) at RT measured in a front face setup.

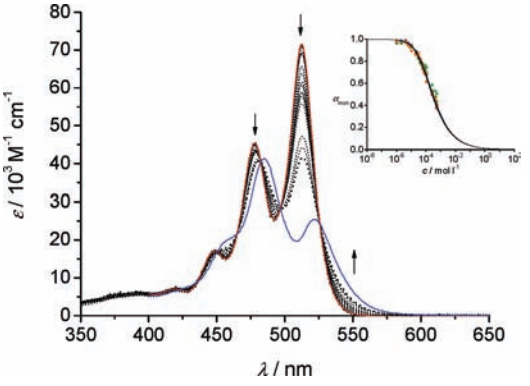

Figure 8. Concentration-dependent UV/vis absorption spectra of (*rac*)-**4b** in *n*-heptane at 331 K ($[M]_0 = 1 \times 10^{-6}$ to 8×10^{-4} M) (dotted lines) and results from the multilinear fit routine showing the derived pure monomer (red) and dimer (blue) spectra. (Inset) Molar fraction of monomer species obtained from nonlinear regression analysis at selected wavelengths. Arrows indicate changes upon increasing concentration.

Supporting Information) to show the possible influence of temperature in the efficiency of chiral self-sorting events. The data obtained at 298 K are collected together with those obtained at 331 K for better comparison (Table 3).

In Figures 8 and S7−S12 in the Supporting Information, concentration-dependent UV/vis studies of (*rac*)-**4b**,**c**, (*P*)-**4b**,**c**, and (*M*)-**4b**,**c** at 331 K in *n*-heptane in a concentration range between 10^{-3} and 10^{-6} M are shown, as well as their fit by nonlinear regression analysis at selected wavelengths and their multilinear fit. Analogous to what was recently reported for **4a**,[5] macrocyclic PBIs **4b** and **4c** show well-defined isosbestic points. Nonlinear regression analysis of the data at selected wavelengths show coherence between the dimerization constants K_D obtained at each wavelength. Moreover, consistent results are obtained through multilinear analysis of the data, which is confirmed by the good accordance between the calculated and the experimental UV/vis spectra at each measured concentration. Due to the larger amount of data processed in the multilinear analysis, we consider these results to be more reliable in comparison to those obtained by single wavelength fit of the data. Therefore, for further analysis, only the K_D values obtained through multilinear routine will be considered.

The results obtained from nonlinear regression analysis at selected wavelength as well as from multilinear regression analysis (Figures 8 and S7−S12 in the Supporting Information) are summarized in Tables S3−S6 in the Supporting Information. The K_D values obtained after multilinear analysis of the concentration-dependent UV/vis data of **4b** and **4c** at 331 and 298 K in *n*-heptane for the quantitative analysis of chiral self-sorting are collected in Table 3 (some data of **4a** already presented in ref 5 are also included for clarity in further discussion).

Applying eq 1[5] to the values collected in Table 3 afforded quantitative information about the ratio of homo and heterochiral

dx.doi.org/10.1021/ja202696d |*J. Am. Chem. Soc.* 2011, 133, 9580–9591

Table 3. Dimerization Constants K_D Determined for (*rac*)-4a−c, (*P*)-4a−c and (*M*)-4a−c in *n*-Heptane at 331 and 298 K by Multilinear Fit of the Concentration-Dependent UV/vis Absorption[a]

sample	T/K	K_D (*P*)[b]/M^{-1}	K_D (*M*)[b]/ M^{-1}	K_D (*rac*)[b]/M^{-1}
4a[c]	331	2800	2800	1500
	298	12 000	12 100	6100
4b	331	5200	5000	3100
	298	18 100	19 700	12 000
4c	331	9100	9300	7000
	298	38 400	39 200	29 900

[a] Values are averaged from two independent data sets. [b] Error of the multilinear analysis is about ±15%. [c] Values for **4a** are taken from ref 5.

Table 4. Dimerization Constants $K_{D(hetero)}$ Obtained From the Values of Table 3 for (*rac*)-4a−c, (*P*)-4a−c and (*M*)-4a−c in *n*-Heptane at 331 and 298 K According to eq 1, the Ratio of Homo- versus Heterodimers Derived Thereof, and Corresponding Percentage of Homodimers Present in Each of the Studied Racemates

sample	T/K	$K_{D(homo)}$[a]/M^{-1}	$K_{D(hetero)}$[a]/M^{-1}	[homo]/[hetero] = $2K_{D(homo)}/K_{D(hetero)}$	% homo
4a	331	2800	400	14.0	93
	298	12 100	200	120.5	99
4b	331	5100	2200	4.6	82
	298	18 900	10 200	3.7	79
4c	331	9200	9600	1.9	66
	298	38 800	42 000	1.8	65
2	331	55000 ± 5400[b]			

[a] Error of the multilinear analysis is about ±15%. [b] See Figure S22 in the Supporting Information.

dimers in a racemic solution (Table 4). The K_D of enantiopure (*P*)-**4a**−**c** (or (*M*)-**4a**−**c**) is related to the formation of homochiral dimers (i.e., $K_D = K_{D(homo)}$), while the obtained $K_{D(rac)}$ from (*rac*)-**4a**−**c** is the average value of homo and hetero dimerization processes.

$$K_{D(rac)} = \frac{K_{D(hetero)} + 2K_{D(homo)}}{4} \qquad (1)$$

The results in Table 4 clearly show that the increasing flexibility from PBIs **4a** to **4c** achieved by the introduction of more extended bridging units between 1 and 7 positions decreases the fidelity of chiral self-recognition in the dimerization process. Thus, upon increasing the bridge length the amount of homochiral dimers present in the racemate decreases from 99−93% in **4a**, to 82−79% in **4b**, and to 66−65% in **4c**. Macrocyclic PBI **4a** with the shortest bridge shows the highest fidelity for chiral self-recognition, which must be directly related to the higher rigidity of its twisted structure. The shortness of the bridge does not allow the twist angle of the PBI core to flip and hence no temporary planar conformation can be achieved, which restricts the stacking possibilities for the dimerization of PBIs **4a**. It has already been shown by CD studies that the twisting angle in the aromatic core region decreases on average upon increasing the length of the bridging unit, which can be explained by a partial planarization of the molecules resulting from the flipping of the naphthalene units, being more pronounced for larger bridges. The flipping process of molecules **4b** and **4c** (being more pronounced for **4c**, due to the larger bridging unit) provides the molecules with more stacking possibilities, some of them allowing a better overlapping of the aromatic surfaces in the heterochiral dimers (temporary planarization and/or flipped structures). These results point to larger amounts of hetero dimers upon increasing the bridge length owing to the flexibility of the molecules, which is associated with a decrease of the average twisting angle of the PBI core. Moreover, the quantity of homochiral dimers at both temperatures for the three studied racemic compounds is nearly the same. In the light of this data, we can conclude that temperature has a very small effect on the fidelity of the chiral self-recognition of **4a**−**c**. This is in good accordance with other reported systems, in which temperature only plays an important role when the thermodynamic equilibrium has not been achieved.[1b,44]

Table 5. Calculated Equilibrium Constants (K') and Related Gibbs Energies ($\Delta G'$) for the Formation of Heterodimers from a Racemic Mixture of Homodimers of 4a−c at 298 and 331 K

T/ K	sample	K'	$\Delta G'$/kJ mol^{-1}
298	**4a**	7×10^{-5}	23.8
	4b	0.073	6.5
	4c	0.293	3.0
331	**4a**	0.005	14.5
	4b	0.047	8.4
	4c	0.272	3.6

It is also notable that the binding constants increase progressively for larger bridging units, being largest for the nonbridged precursor **2**. From **4a** to **4b** and from **4b** to **4c**, the binding constants double for each successive increase of the OEG bridge length. This trend is lost for precursor **2**, which has a much higher binding constant than **4c** (about six times higher than $K_{D(homo)}$ and eight times higher than $K_{D(rac)}$). This progression can be rationalized by the induced-fit effect, by which the PBIs undergo an appreciable change in their three-dimensional structure upon formation of a π-stacked dimer. The extent of the induced fit is directly related to the flexibility of the molecules. The most flexible molecule, precursor **2**, is able to accomplish the most pronounced structural changes to fit the other PBI molecule within the dimer complex. The tremendous difference between the binding constants of **2** and (*rac*)-**4c** (Table 3) can be explained by three features of molecule **2**: (i) the presence of two free π-surfaces available for π−π-stacking (purely entropic contribution), (ii) the possibility of complete flipping of the naphthalene units from *M* to *P* atropo-enantiomers, and (iii) the possibility of the phenoxy groups attached to the 1,7-bay positions to freely rotate and adopt the most favorable conformation to stabilize the self-assembled π-stack. The conformational changes of these phenoxy units are considerably limited by the presence of the OEG bridges, thus only the effect of the more or less restricted flipping of the naphthalene units will contribute to the induced fit process for the dimerization process of **4a**−**c**. Consequently, the increasing flexibility in PBI aromatic cores has a positive influence on the induced-fit effects in the dimerization process as reflected in the calculated binding constants, while it clearly compromises the quality of the chiral self-sorting process.

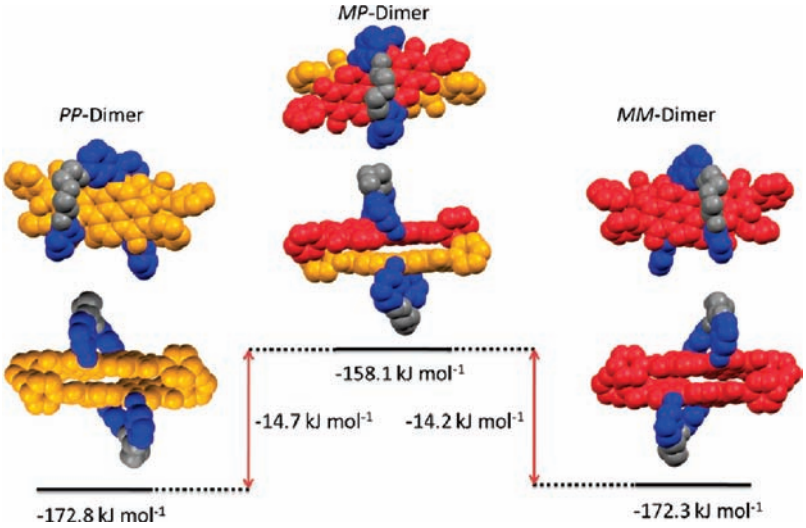

Figure 9. Energy diagram of the different supramolecular diastereomers of **4a**. The OEG are represented in gray, the phenoxy units in blue, and the PBI core in red for *M*-enantiomer and yellow for *P*-enantiomer.

Equilibrium Constant *K′* for the Formation of Heterodimers from Homodimers. The equilibrium constant (K') and related Gibbs energy ($\Delta G'$) for the formation of heterodimers from a racemic mixture of homodimers can be calculated applying the values obtained for $K_{D(homo)}$ and $K_{D(hetero)}$ into eq 2, and the obtained K' into $\Delta G' = -RT \ln K'$ (where R is the ideal gas constant and T is the temperature in Kelvin). The calculated values for **4a**−**c** at 298 and 331 K are summarized in Table 5.[5]

$$4K' = \frac{K^2_{D(hetero)}}{K^2_{D(homo)}} \qquad (2)$$

The data in Table 5 show that $\Delta G'$ values are steadily positive for the whole series. Thus, the formation of heterodimers from the respective homodimers remains in all cases a disfavored process. The highest fidelity of chiral self-recognition, i.e. preference for homo versus heterodimer formation, is found for the shortest bridging unit. Upon increasing the bridge length and hence the flexibility of the structures of **4a**−**c**, the formation of heterodimers becomes energetically less unfavorable, enabling an increasing amount of heterochiral dimers in the racemic solution. The tendency shown by these data anticipates that a long enough bridging unit might provide a system in which the formation of heterodimers is favored (for entropic reasons) over the formation of homodimers, or at least equally favorable.

For a better understanding of the experimental results, DFT structure optimization of homo and heterodimers formed by **4a** were performed at the RI-BLYP-D/TZV(P) level (cf. Computational Details). For the different diastereomers (*MM*, *PP* and *MP*) two different structure types with energetically similar minima could be found (Figure S23 in the Supporting Information). One of the structures shows an ecliptic arrangement, with the PBIs almost superimposed and very small rotational displacement (Figure S23a in the Supporting Information). The second, marginally less favored structure exhibits two stacked PBIs with rotational displacement of about 30° (Figure S23b in the Supporting Information). The latter arrangement is consistent with previous experimental and theoretical results for unsubstituted PBIs[27] in their ground state, and with our CD data at high concentrations in *n*-hexane, whose bisignate Cotton effects indicate the presence of dimers with rotational displacements. Thus, only these dimeric species will be considered for further discussion (the preference for the eclipsed structure in the computation by 5 kJ mol^{-1} is entirely due to a larger dispersion contribution of about 15 kJ mol^{-1}, whereas the rotated structure is favored by electrostatics[27]).

The energies obtained for both homochiral dimers are, as expected, equal within possible errors arising from incompleteness of structure optimization convergence on very shallow potential energy surfaces (Figure 9). The computed dimerization energy for the rotated homochiral dimer is ca. 173 kJ mol^{-1}, which is larger than obtained previously at the same level for an unsubstituted PBI dimer (125 kJ mol^{-1}).[27] The heterochiral dimer was calculated to be 14.5 kJ mol^{-1} (19.2 kJ mol^{-1} for the ecliptic conformer) less stable than the homodimers in excellent accordance with the experimental values (Table 5), supporting the validity of the calculations. Thus, the higher stability of homochiral dimers over their heterochiral counterparts has been demonstrated both experimentally and theoretically. The reason of this extra stabilization in the case of the homodimers is clearly the better overlapping of the π-surfaces in comparison to the heterochiral dimers as can be appreciated from Figure 9. The better fit between the, in this case self-complementary aromatic surfaces of the homodimer is apparent. The heterodimer exhibits less tight $\pi-\pi$-stacking and some distortion of the monomer structures in the dimer (Figure 9). Such geometrical factors have been previously proven to be decisive in the efficiency of both chiral and "general" self-sorting processes.[13c,16b,45]

■ CONCLUSIONS

This series of core-twisted dyes enabled for the first time the elucidation of the effect of conformational parameters (rigidity of a chiral π-scaffold) on binding constants for dimerization by $\pi-\pi$-stacking and selectivity of chiral recognition (homo- versus heterochiral dimerization). Already CD spectra of monomeric pure enantiomers revealed a greater flexibility of the PBI structures equipped with larger bridging units owing to a more pronounced flipping of the chiral PBI scaffold. Concentration-dependent

dx.doi.org/10.1021/ja202696d | *J. Am. Chem. Soc.* 2011, 133, 9580–9591

spectroscopic studies of racemic and enantiopure PBI dyes **4a**−**c** provided unambiguous evidence for preferential chiral self-recognition over self-discrimination in π-stacking dimerization of these PBIs. However, the amount of heterochiral dimers present in the corresponding racemates increases for more extended bridging units. This demonstrates that the fidelity of chiral self-sorting in PBIs is compromised by an increasing flexibility of the structures. Less rigid scaffolds bearing longer bridging units were shown to enable more planarized π-scaffolds upon $\pi-\pi$-stacking by means of a induced-fit mechanism leading to higher binding strength but lower enantioselectivity for the recognition of the homo or heterochiral partner molecule.

To conclude, we have revealed for the first time the impact of rigidity on chiral self-sorting processes for core-twisted π-scaffolds. Conformational flexibility was shown to improve the binding strength via induced-fit mechanism but at the expense of the quality of chiral self-recognition between chiral π-surfaces.

■ ASSOCIATED CONTENT

Supporting Information. ^{1}H NMR spectra of new compounds, additional UV/vis spectra and binding constants, and X-ray crystallographic data for (*P*)-**3a**. This material is available free of charge via the Internet at http://pubs.acs.org.

■ AUTHOR INFORMATION

Corresponding Author
wuerthner@chemie.uni-wuerzburg.de

■ ACKNOWLEDGMENT

We acknowledge financial support from the DFG (GRK 1221).

■ REFERENCES

(1) (a) Kramer, R.; Lehn, J. M.; Marquisrigault, A. *Proc. Natl. Acad. Sci. U.S.A.* **1993**, *90*, 5394–5398. (b) Wu, A. X.; Isaacs, L. *J. Am. Chem. Soc.* **2003**, *125*, 4831–4835. (c) Mukhopadhyay, P.; Wu, A. X.; Isaacs, L. *J. Org. Chem.* **2004**, *69*, 6157–6164. (d) Shivanyuk, A.; Rebek, J., Jr. *J. Am. Chem. Soc.* **2002**, *124*, 12074–12075. (e) Taylor, P. N.; Anderson, H. L. *J. Am. Chem. Soc.* **1999**, *121*, 11538–11545. (f) Jiang, W.; Winkler, H. D. F.; Schalley, C. A. *J. Am. Chem. Soc.* **2008**, *130*, 13852–13853.

(2) (a) Corbett, P. T.; Sanders, J. K. M.; Otto, S. *Angew. Chem., Int. Ed.* **2007**, *46*, 8858–8861. (b) Ludlow, R. F.; Otto, S. *Chem. Soc. Rev.* **2008**, *37*, 101–108. (c) Peyralans, J. J. P.; Otto, S. *Curr. Opin. Chem. Biol.* **2009**, *13*, 705–713. (d) Nitschke, J. R. *Nature* **2009**, *462*, 736–738. (e) Wagner, N.; Ashkenasy, G. *J. Chem. Phys.* **2009**, 16907 (1).

(3) (a) Kühnle, A.; Linderoth, T. R.; Hammer, B.; Besenbacher, F. *Nature* **2002**, *415*, 891–893. (b) Huang, W. H.; Zavalij, P. Y.; Isaacs, L. *Angew. Chem., Int. Ed.* **2007**, *46*, 7425–7427. (c) Zehnacker, A.; Suhm, M. A. *Angew. Chem., Int. Ed.* **2008**, *47*, 6970–6992.

(4) (a) Pasteur, L. C. R. *Hebd. Seanc. Acad. Sci.* **1848**, *26*, 538. (b) Kondepudi, D. K.; Kaufman, R. J.; Singh, N. *Science* **1990**, *250*, 975–976. (c) Crusats, J.; Veintemillas-Verdaguer, S.; Ribó, J. M. *Chem.—Eur. J.* **2006**, *12*, 7776–7781. (d) Fletcher, S. P.; Jagt, R. B. C.; Feringa, B. L. *Chem. Commun.* **2007**, 2578–2580. (e) Blackmond, D. G. *Chem.—Eur. J.* **2007**, *13*, 3290–3295. (f) McBride, J. M.; Tully, J. C. *Nature* **2008**, *452*, 161–162.

(5) Safont-Sempere, M. M.; Osswald, P.; Radacki, K.; Würthner, F. *Chem.—Eur. J.* **2010**, *16*, 9366–9373.

(6) Würthner, F. *Chem. Commun.* **2004**, 1564–1579.

(7) (a) Zhan, X. W.; Facchetti, A.; Barlow, S.; Marks, T. J.; Ratner, M. A.; Wasielewski, M. R.; Marder, S. R. *Adv. Mater.* **2011**, *23*, 268–284. (b) Letizia, J. A.; Rivnay, J.; Facchetti, A.; Ratner, M. A.; Marks, T. J. *Adv. Funct. Mater.* **2010**, *20*, 50–58. (c) Weil, T.; Vosch, T.; Hofkens, J.; Peneva, K.; Müllen, K. *Angew. Chem., Int. Ed.* **2010**, *49*, 9068–9093.

(8) (a) Schmidt, R.; Oh, J. H.; Sun, Y. S.; Deppisch, M.; Krause, A. M.; Radacki, K.; Braunschweig, H.; Könemann, M.; Erk, P.; Bao, Z. A.; Würthner, F. *J. Am. Chem. Soc.* **2009**, *131*, 6215–6228. (b) Sautter, A.; Thalacker, C.; Würthner, F. *Angew. Chem., Int. Ed.* **2001**, *40*, 4425–4429. (c) Jones, B. A.; Ahrens, M. J.; Yoon, M. H.; Facchetti, A.; Marks, T. J.; Wasielewski, M. R. *Angew. Chem., Int. Ed.* **2004**, *43*, 6363–6366. (d) Chen, Z.; Debije, M. G.; Debaerdemaeker, T.; Osswald, P.; Würthner, F. *ChemPhysChem* **2004**, *5*, 137–140. (e) Würthner, F.; Stepanenko, V.; Chen, Z.; Saha-Möller, C. R.; Kocher, N.; Stalke, D. *J. Org. Chem.* **2004**, *69*, 7933–7939. (f) Leroy-Lhez, S.; Baffreau, J.; Perrin, L.; Levillain, E.; Allain, M.; Blesa, M. J.; Hudhomme, P. *J. Org. Chem.* **2005**, *70*, 6313–6320. (g) Chao, C. C.; Leung, M. K.; Su, Y. O.; Chiu, K. Y.; Lin, T. H.; Shieh, S. J.; Lin, S. C. *J. Org. Chem.* **2005**, *70*, 4323–4331. (h) Würthner, F.; Osswald, P.; Schmidt, R.; Kaiser, T. E.; Mansikkamaki, H.; Könemann, M. *Org. Lett.* **2006**, *8*, 3765–3768.

(9) (a) Xiao, S.; Myers, M.; Miao, Q.; Sanaur, S.; Pang, K.; Steigerwald, M. L.; Nuckolls, C. *Angew. Chem., Int. Ed.* **2005**, *44*, 7390–7394. (b) Fasel, R.; Parschau, M.; Ernst, K. H. *Nature* **2006**, *439*, 449–452. (c) Phillips, K. E. S.; Katz, T. J.; Jockusch, S.; Lovinger, A. J.; Turro, N. J. *J. Am. Chem. Soc.* **2001**, *123*, 11899–11907.

(10) Gsänger, M.; Oh, J. H.; Könemann, M.; Hoffken, H. W.; Krause, A. M.; Bao, Z. N.; Würthner, F. *Angew. Chem., Int. Ed.* **2010**, *49*, 740–743.

(11) (a) Xie, Z.; Würthner, F. *Org. Lett.*, **2010**, *12*, 3204−3207. (b) Osswald, P.; Würthner, F. *J. Am. Chem. Soc.* **2007**, *129*, 14319–14326.

(12) (a) Osswald, P.; Leusser, D.; Stalke, D.; Würthner, F. *Angew. Chem., Int. Ed.* **2005**, *44*, 250–253. (b) Osswald, P.; Reichert, M.; Bringmann, G.; Würthner, F. *J. Org. Chem.* **2007**, *72*, 3403–3411.

(13) (a) Hwang, I. W.; Kamada, T.; Ahn, T. K.; Ko, D. M.; Nakamura, T.; Tsuda, A.; Osuka, A.; Kim, D. *J. Am. Chem. Soc.* **2004**, *126*, 16187–16198. (b) Kamada, T.; Aratani, N.; Ikeda, T.; Shibata, N.; Higuchi, Y.; Wakamiya, A.; Yamaguchi, S.; Kim, K. S.; Yoon, Z. S.; Kim, D.; Osuka, A. *J. Am. Chem. Soc.* **2006**, *128*, 7670–7678. (c) Mizumura, M.; Shinokubo, H.; Osuka, A. *Angew. Chem., Int. Ed.* **2008**, *47*, 5378–5381. (d) Maeda, C.; Kamada, T.; Aratani, N.; Sasamori, T.; Tokitoh, N.; Osuka, A. *Chem.—Eur. J.* **2009**, *15*, 9681–9684.

(14) (a) Sugiyasu, K.; Honsho, Y.; Harrison, R. M.; Sato, A.; Yasuda, T.; Seki, S.; Takeuchi, M. *J. Am. Chem. Soc.* **2010**, *132*, 14754–14756. (b) Sugiyasu, K.; Takeuchi, M. *Chem.—Eur. J.* **2009**, *15*, 6350–6362.

(15) (a) Long, T. M.; Swager, T. M. *J. Mater. Chem.* **2002**, *12*, 3407–3412. (b) Lohr, A.; Swager, T. M. *J. Mater. Chem.* **2010**, *20*, 8107–8111. (c) Lim, J.; Swager, T. M. *Angew. Chem., Int. Ed.* **2010**, *49*, 7486–7488.

(16) (a) Wang, W.; Shaller, A. D.; Li, A. D. Q. *J. Am. Chem. Soc.* **2008**, *130*, 8271–8279. (b) Shaller, A. D.; Wang, W.; Gan, H. Y.; Li, A. D. Q. *Angew. Chem., Int. Ed.* **2008**, *47*, 7705–7709.

(17) (a) Thoma, J. A.; Koshland, D. E., Jr. *J. Am. Chem. Soc.* **1960**, *82*, 3329–3333. (b) Koshland, D. E. *Angew. Chem., Int. Ed.* **1995**, *33*, 2375–2378.

(18) (a) James, L. C.; Roversi, P.; Tawfik, D. S. *Science* **2003**, *299*, 1362–1367. (b) Martin Schmeing, T.; Huang, K. S.; Strobel, S. A.; Steitz, T. A. *Nature* **2005**, *438*, 520–524. (c) Ringe, D.; Petsko, G. A. *Science* **2008**, *320*, 1428–1429.

(19) (a) Kasai, K.; Aoyagi, M.; Fujita, M. *J. Am. Chem. Soc.* **2000**, *122*, 2140–2141. (b) Gasparrini, F.; Pierini, M.; Villani, C.; Filippi, A.; Speranza, M. *J. Am. Chem. Soc.* **2007**, *130*, 522–534. (c) Filby, M. H.; Dickson, S. J.; Zaccheroni, N.; Prodi, L.; Bonacchi, S.; Montalti, M.; Paterson, M. J.; Humphries, T. D.; Chiorboli, C.; Steed, J. W. *J. Am. Chem. Soc.* **2008**, *130*, 4105–4113. (d) Hiraoka, S.; Harano, K.; Nakamura, T.; Shiro, M.; Shionoya, M. *Angew. Chem., Int. Ed.* **2009**, *48*, 7006–7009. (e) Ménand, M.; Leroy, A.; Marrot, J.; Luhmer, M.; Jabin, I. *Angew. Chem., Int. Ed.* **2009**, *48*, 5509–5512. (f) Han, J.-M.; Pan, J.-L.; Lei, T.; Liu, C.; Pei, J. *Chem.—Eur. J.* **2010**, *16*, 13850–13861.

(20) Marquis, D.; Desvergne, J. P.; Bouaslaurent, H. *J. Org. Chem.* **1995**, *60*, 7984–7996.

(21) (a) Hwang, T. L.; Shaka, A. J. *J. Am. Chem. Soc.* **1992**, *114*, 3157–3159. (b) Hwang, T. L.; Kadkhodaei, M.; Mohebbi, A.; Shaka, A. J. *Magn. Reson. Chem.* **1992**, *30*, 24–34.

(22) Sheldrick, G. *Acta Crystallogr.* **2008**, *A64*, 112–122.

(23) (a) Gvishi, R.; Reisfeld, R.; Burshtein, Z. *Chem. Phys. Lett.* **1993**, *213*, 338–344. (b) Sens, R.; Drexhage, K. H. *J. Lumin.* **1981**, *24*−*5*, 709–712.

(24) Ahlrichs, R.; Bär, M.; Häser, M.; Horn, H.; Köhmel, C. *Chem. Phys. Lett.* **1989**, *162*, 165.

(25) (a) Becke, A. D. *Phys. Rev. A* **1988**, *38*, 3098–3100. Lee, C.; Yang, W.; Parr, R. G. *Phys. Rev. B: Condens. Matter Mater. Phys.* **1988**, *37*, 785–789. (b) Treutler, O.; Ahlrichs, R. *J. Chem. Phys.* **1995**, *102*, 346–354. (c) Schäfer, A.; Huber, C.; Ahlrichs, R. *J. Chem. Phys.* **1994**, *100*, 5829–5835. (d) Eichkorn, K.; Weigend, F.; Treutler, O.; Ahlrichs, R. *Theor. Chim. Acta* **1997**, *97*, 119–124.

(26) (a) Grimme, S. *J. Comput. Chem.* **2004**, *25*, 1463–1473. See also(b) Piacenza, M.; Grimme, S. *ChemPhysChem* **2005**, *6*, 1554. (c) Antony, J.; Grimme, S. *Phys. Chem. Chem. Phys.* **2006**, *8*, 5287–5297. (d) Grimme, S.; Antony, J.; Schwabe, T.; Mück-Lichtenfeld, C. *Org. Biomol. Chem.* **2007**, *5*, 741–745.

(27) (a) Fink, R. F.; Seibt, J.; Engel, V.; Renz, M.; Kaupp, M.; Lochbrunner, S.; Zhao, H.-M.; Pfister, J.; Würthner, F.; Engels, B. *J. Am. Chem. Soc.* **2008**, *130*, 12858–12859. (b) Zhao, H.-M.; Pfister, J.; Settels, V.; Renz, M.; Kaupp, M.; Dehm, V. C.; Würthner, F.; Fink, R. F.; Engels, B. *J. Am. Chem. Soc.* **2009**, *131*, 15660–15668.

(28) Marquis, D.; Desvergne, J. P.; Bouaslaurent, H. *J. Org. Chem.* **1995**, *60*, 7984–7996.

(29) Dijkstra, G.; Kruizinga, W. H.; Kellogg, R. M. *J. Org. Chem.* **1987**, *52*, 4230–4234.

(30) Kaiser, H.; Lindner, J.; Langhals, H. *Chem. Ber.* **1991**, *124*, 529–535.

(31) For the details on the determination of absolute configurations of similar PBI marcocycles see ref. 12b.

(32) Fron, E.; Schweitzer, G.; Osswald, P.; Würthner, F.; Marsal, P.; Beljonne, D.; Müllen, K.; De Schryver, F. C.; Van der Auweraer, M. *Photochem. Photobiol. Sci.* **2008**, *7*, 1509–1521.

(33) (a) Klebe, G.; Graser, F.; Hadicke, E.; Berndt, J. *Acta Crystallogr., Sect. B: Struct. Sci* **1989**, *45*, 69–77. (b) Hino, K.; Mizuguchi, J. *Acta Crystallogr., Sect. E: Struct. Rep. Online* **2005**, *61*, O672–O674.

(34) (a) Bergman, S. D.; Kol, M. *Inorg. Chem.* **2005**, *44*, 1647–1654. (b) Gut, D.; Rudi, A.; Kopilov, J.; Goldberg, I.; Kol, M. *J. Am. Chem. Soc.* **2002**, *124*, 5449–5456. (c) Giordano, C.; Restelli, A.; Villa, M.; Annunziata, R. *J. Org. Chem.* **1991**, *56*, 2270–2272. (d) Luchinat, C.; Roelens, S. *J. Am. Chem. Soc.* **1986**, *108*, 4873–4878. (e) Dobashi, A.; Saito, N.; Motoyama, Y.; Hara, S. *J. Am. Chem. Soc.* **1986**, *108*, 307–308. (f) Harger, M. J. P. *J. Chem. Soc., Perkin Trans. 2* **1977**, 1882–1887.

(35) As COSY experiments are much more sensitive than ROESY ones, if the cross peak signal arises from an intramolecular coupling of the protons, it must be present in both ROESY and COSY spectra. As it is not the case, this cross peak must be originated intermolecularly.

(36) Such studies are not possible for macrocycles **3a**−**c** due to poor solubility at the required concentrations in nonpolar solvents.

(37) Chen, Z.; Baumeister, U.; Tschierske, C.; Würthner, F. *Chem.—Eur. J.* **2007**, *13*, 450–465.

(38) (a) Berova, N.; Nakanishi, K. *Circular Dichroism: Principles and Applications*; Wiley-VCH: New York, 2000. (b) Berova, N.; Di Bari, L.; Pescitelli, G. *Chem. Soc. Rev.* **2007**, *36*, 914–931. (c) Buss, V.; Reichardt, C. *Chem. Commun.* **1992**, 1636–1638.

(39) (a) Rybtchinski, B.; Sinks, L. E.; Wasielewski, M. R. *J. Phys. Chem. A* **2004**, *108*, 7497–7505. (b) Ahrens, M. J.; Sinks, L. E.; Rybtchinski, B.; Liu, W. H.; Jones, B. A.; Giaimo, J. M.; Gusev, A. V.; Goshe, A. J.; Tiede, D. M.; Wasielewski, M. R. *J. Am. Chem. Soc.* **2004**, *126*, 8284–8294. (c) van der Boom, T.; Hayes, R. T.; Zhao, Y. Y.; Bushard, P. J.; Weiss, E. A.; Wasielewski, M. R. *J. Am. Chem. Soc.* **2002**, *124*, 9582–9590. (d) Giaimo, J. M.; Gusev, A. V.; Wasielewski, M. R. *J. Am. Chem. Soc.* **2002**, *124*, 8530–8531.

(40) (a) Würthner, F.; Chen, Z.; Dehm, V.; Stepanenko, V. *Chem. Commun.* **2006**, 1188–1190. (b) Tolkki, A.; Vuorimaa, E.; Chukharev, V.; Lemmetyinen, H.; Ihalainen, P.; Peltonen, J.; Dehm, V.; Würthner, F. *Langmuir* **2009**, *26*, 6630–6637.

(41) Yoo, H.; Yang, J.; Yousef, A.; Wasielewski, M. R.; Kim, D. *J. Am. Chem. Soc.* **2010**, *132*, 3939–3944.

(42) (a) Connors, K. A. *Binding Constants: The Measurement of Molecular Complex Stability*; Wiley: New York, 1987. (b) Lagona, J.; Mukhopadhyay, P.; Chakrabarti, S.; Isaacs, L. *Angew. Chem., Int. Ed.* **2005**, *44*, 4844–4870.

(43) Wortmann, R.; Rösch, U.; Redi-Abshiro, M.; Würthner, F. *Angew. Chem., Int. Ed.* **2003**, *42*, 2080–2083.

(44) Zheng, Y. R.; Yang, H. B.; Ghosh, K.; Zhao, L.; Stang, P. J. *Chem.—Eur. J.* **2009**, *15*, 7203–7214.

(45) (a) Amemiya, R.; Yamaguchi, M. *Org. Biomol. Chem.* **2008**, *6*, 26–35. (b) Trzaska, S. T.; Hsu, H. F.; Swager, T. M. *J. Am. Chem. Soc.* **1999**, *121*, 4518–4519.